IL NUOVO CIMENTO VOL. 23 C, N. 2 Marzo-Aprile 2000

A numerical study of optical and physical properties of mixed-phase polar stratospheric clouds

G. P. GOBBI (*)
Istituto di Fisica dell'Atmosfera, Consiglio Nazionale delle Ricerche
Via Fosso del Cavaliere 100, 00133 Roma, Italy

(ricevuto il 19 Ottobre 1998; approvato il 10 Gennaio 2000)

Summary. — A numerical model designed to describe the microphysics of stratospheric aerosols along an isentropic trajectory is employed to study optical and physical properties of mixed-phase polar stratospheric clouds (PSC). Particles size distribution is studied following the evolution of 1000 size bins. Solid particles are assumed to first form upon homogeneous nucleation of water ice. Heterogeneous formation of nitric acid trihydrate (NAT) and sulphuric acid tetrahydrate (SAT) is then assumed to take place only on the homogeneously nucleated ice particles. Two cooling rates, 10 K/day and 1000 K/day, representative in turn of synoptic and wave cooling events are employed. These lead to the nucleation of 0.1% and 80% of ambient aerosols, respectively. Following nucleation, the time evolution of PSC optical and physical properties is shown to be strongly influenced by the number of nucleated particles. The model-derived lidar backscatter ratio, depolarization ratio and extinction (all at 532 nm), plus distribution surface area and effective radius of equilibrium and non-equilibrium PSC are presented. These results provide links between polarization lidar observations and PSC composition and phase.

PACS 92.60.Mt – Particles and aerosols.
PACS 94.10.Gb – Absorption and scattering of radiation.

1. – Introduction

The role of polar stratospheric clouds (PSC) in the springtime depletion of ozone at high latitudes has been well defined during the past decade. PSC form in the winter stratosphere by temperature-driven condensation of ambient nitric acid and water onto background sulphate aerosols. Heterogeneous chemistry reactions developing on the surface of PSC particles then activate ambient halogenated species (chlorine and

(*) E-mail: gobbi@ifa.rm.cnr.it

bromine compounds) which catalitically destroy ozone in the presence of sunlight. At the same time, settling of the largest PSC particles removes the nitrates (NO_y) which would interrupt the ozone destruction cycles by recombining with the activated halogens [1].

In stratospheric conditions, nitric acid/water mixtures condense at temperatures higher than pure water does. At 50 hPa and in the presence of a typical mixing ratio of 4 ppmv H_2O, the ice frost point is $T_f \approx 187$ K. Most of the ambient nitric acid (typically 10 ppbv) condenses onto background aerosols (supercooled solutions of sulphuric acid and water) starting at approximately 190 K and leading to the formation of supercooled ternary solutions (STS) of H_2SO_4, HNO_3 and water [2]. Conversely, nitric acid trihydrate (NAT), the most stable form of frozen nitric acid, has an equilibrium temperature of approximately 195 K [3]. HNO_3 vapor pressures are then much lower over NAT than over STS. Nevertheless, NAT is not frequently observed, particularly at the beginning and end of winter or when temperatures do not remain very low for long periods [4]. A likely explanation for this behaviour resides in the fact that formation of NAT requires a nucleation process, and laboratory work [5] showed that such nucleation can proceed along with the formation of several metastable solid hydrates of HNO_3 and H_2SO_4, before achieving the final crystallization of NAT. Sulphuric acid tetra-hydrate (SAT) and nitric acid di-hydrate (NAD) represent two relevant steps of such a nucleation pattern. In this respect, observations of lee-wave PSC reported nitric acid solid hydrates to nucleate and slowly grow in airmasses where ice formed first [6]. Since the nucleation sequence generated by a slow cooling can take place on timescales in excess of 24 hours, warmings which may occur meanwhile can lead to the evaporation of the metastable phases before NAT is formed.

In the following sections, it will be shown that even after formation of NAT, diffusion transfer times of HNO_3 from STS droplets to NAT crystals can be quite long if NAT nucleated out of a small fraction of ambient aerosols. Such a condition, leading to the formation of mixed-phase PSC (an external mixture of liquid and solid particles in the same air volume) is often encountered in the winter polar stratosphere [7, 8]. Mixed phases containing STS and solid HNO_3 or ice have both been observed in the Antarctic stratosphere [9]. A similar pattern of homogeneous nucleation characterizes cirrus clouds, where typically 1 out of 1000 ambient aerosol particles nucleate an ice crystal [10].

This paper will present optical properties of STS, SAT, NAT, and ice mixed-phase PSC, as obtained by means of a numerical model simulating aerosol microphysics. Different cooling rates, leading to differing amounts of nucleated particles, will be addressed. Backscatter and depolarization of both non-equilibrium and equilibrium PSC will be analyzed to provide typical values of these parameters for STS, SAT, NAT and ice PSC. These results provide a means to estimate PSC composition and phase on the basis of polarization lidar observations at 532 nm. Recently, other model simulations of physical and optical properties of non-equilibrium PSC have appeared in the literature [11, 12, 6]. These numerical experiments did not specifically simulate nucleation, they investigated only fast cooling events and considered size distributions discretized over 26 size bins. The numerical simulations presented here differ from the previous ones because the model employed in this work: a) simulates aerosol homogeneous nucleation; b) addresses both fast and slow cooling airmasses; c) computes PSC microphysical and optical properties following the evolution of the aerosol size distribution discretized into 1000 bins, improving therefore the quality of available estimates of PSC characteristics.

2. – Outline of the model

The aerosol "box" model (ABM) employed in this study simulates the isentropic evolution of a 1 cm^3 air parcel along a prescribed temperature history. The ABM takes into account nucleation and diffusional growth of binary (H_2SO_4-H_2O), ternary (H_2SO_4-HNO_3-H_2O), SAT, NAT and ice particles. The initial air parcel contains typical stratospheric amounts of background gases and sulphate aerosols. The background aerosol size distribution is described by a lognormal curve with number density $N_0 = 10\ cm^{-3}$, mode radius $r_g = 7.25 \times 10^{-6}$ cm and width $\sigma = 1.86$, according to [13]. This size distribution is digitized over 1000 size bins, logarithmically spaced over the 4-decade interval 0.01–100 μm. Choice of the 250 bins/decade resolution was made after assessing that convergence in the integration of optical properties took place past this resolution. For each bin the model keeps track of the size, composition, phase and molecular content in H_2SO_4, HNO_3 and H_2O. The formulation of gas diffusion between the atmosphere and the particles is equivalent to the one already presented in [14], *i.e.*, it includes Kelvin effect, Knudsen correction to the diffusion coefficients and particle temperature adjustment due to latent heat variations. The reader is referred to such publication for further details. Vapor pressures of individual species over the relevant solid are derived from the following sources: H_2SO_4 vapor pressures over binary solutions are computed according to Hamill (personal communication, 1995); HNO_3 vapor pressures and composition of STS are obtained according to [2], while ref. [3] is the source of HNO_3 vapor pressures over NAT and H_2O vapor pressures over ice are derived from [10].

Simulating nucleation is a weak point in all cloud models. PSC represent no exception. Cirrus clouds likely form via a homogeneous nucleation process [15] and ice PSC seem to follow a similar behaviour, nucleating approximately 2 K below the ice frost point [6]. Conversely, appearance of HNO_3-based solids is commonly observed well below the NAT equilibrium temperature, see, *e.g.*, [4]. As mentioned in the introduction, NAT nucleation might take place along a pattern lasting many hours and involving sequential formation of several hydrates. Presently no theory is available to describe such a process. On the other hand, PSC observations show alternatively the action of both selective nucleation and of nucleation of the majority of ambient particles. The latter case is most likely to occur in fast cooling airmasses, *i.e.*, when large supersaturations allow quasi-simultaneous overtaking of nucleation barriers at all sizes [16]. Recent observations [6] showed ice PSC to homogeneously nucleate out of 50–100% of ambient aerosols during fast, lee-wave coolings. After ice evaporation upon warming, these observations indicated that nitric acid hydrates had also nucleated. Formation of sulphuric acid hydrates could not be observed because temperature never rose above NAT equilibrium during these measurements. In this respect, the nucleation mechanisms of SAT remains poorly known, even though backscatter compatible with sulphuric acid solid hydrates is very common in polar winter observations [9].

In order to reproduce the PSC formation constraints discussed above, the model simulations presented here prescribe that no solid particles form before homogeneous nucleation of ice takes place. The model then imposes that all other molecules in a STS droplet aggregate into the relevant stable crystals (SAT or NAT) when ice nucleation is reached by that droplet, *i.e.*, SAT or NAT immediately form out of the nitric acid and sulphuric acid molecules present in the size bins where ice nucleates. This is equivalent to assuming that there are no barriers to the heterogeneous nucleation of NAT and

SAT on ice crystals. Naturally, SAT, NAT and ice particles then melt or evaporate only when reaching above the relevant stability temperature.

Homogeneous nucleation rates are computed according to the formulation provided in eq. 4.12 of ref. [17]. Test simulations showed that in STS, homogeneous nucleation of ice takes place approximately 2 K above the temperature at which NAT nucleates. Homogeneous nucleation rates and gas-to-particle diffusion are computed employing time steps down to 0.1 s, depending on the level of supersaturation. Particle coagulation is not considered because of its minor effects on PSC [16].

The model computes optical parameters such as extinction, lidar parallel backscatter ratio $R = 1 + (\beta_{a\parallel} / \beta_{m\parallel})$ and depolarization ratio $D = (\beta_{a\perp} + \beta_{m\perp}) / (\beta_{a\parallel} + \beta_{m\parallel})$ at 532 nm, plus surface and volume of both liquid and solid particles in the distribution. In the previous formulae β_a and β_m represent the aerosol and molecular backscatter cross-sections, respectively. These two quantities are obtained from the combined analysis of the lidar trace and of the air density profile. The symbols $\parallel$ and $\perp$ indicate laser-referred parallel and perpendicular polarization of received signals, respectively. It should be noticed that the air mass total depolarization ratio employed here differs from the aerosol depolarization ratio $D_A = = \beta_{a\perp} / \beta_{a\parallel}$ (which represents the average depolarization of spherical and non-spherical aerosol particles alone) used in [18]. However, D is more commonly employed in lidar analysis. In this respect readers should be aware that the definition of lidar parameters often differs from author to author and some care should be taken in comparing different lidar observations.

Extinction and backscatter cross-sections are computed in the ABM by means of the Mie theory, *i.e.*, assuming particles are spherical. The model depolarization ratio D is computed prescribing that a fixed fraction (33%) of the backscatter from frozen particles is depolarized into the perpendicular channel and, accordingly with the Mie theory, no depolarization is generated by spherical aerosols. This parameterization is justified by the observation of a quasi-constant depolarization ratio $D_c = \beta_{c\perp} / \beta_{c\parallel} \approx 0.50$, *i.e.*, $\beta_{c\perp} \approx 0.33\, \beta_c$, characterizing lidar observations of simple crystals and PSC, see, *e.g.*, [19, 9]. In the case of size distributions with effective radius $r_{eff} > 0.5$ μm, such an assumption is also supported by some of the theoretical calculations of [20]. Results presented here will show that PSC are mostly characterized by $r_{eff} > 0.5$ μm.

3. – Discussion of model results

The initial temperature and pressure of the simulated air mass are $T = 198$ K and $p = 50$ hPa, respectively. Typical early winter, lower polar stratosphere mixing ratios of 4 ppmv for water and 10 ppbv for nitric acid are employed. In these conditions, SAT, NAT and ice freezing points are $T_{SAT} \approx 205$–210 K, $T_{NAT} = 195$ K, and $T_f = 187.5$ K, respectively. Two cooling rates, a) 1000 K/day, and b) 10 K/day, have been employed to study the effects of homogeneous nucleation on selective growth of particles. These two cases bracket the variability range observed in the upper troposphere and lower stratosphere, during extensive temperature measurements [21], and are representative of synoptic and lee-wave nucleation events. While detailed results of numerical simulations are plotted in fig. 1, typical optical and physical properties of various PSC compositions and mixtures at equilibrium as obtained by the ABM are summarized in table I. For comparison purposes, some parameters obtained in simulations addressing the case of a dehydrated (2 ppmv H_2O) and denitrified (2 ppbv HNO_3) stratosphere [22] are also included in table I. In this case, the temperature history was approximately

TABLE I. – *Equilibrium values of aerosol parameters for various PSC compositions* (*).

Time (h)	T (K)	NUC (%)	R	D (%)	r_{eff} (μm)	EXT (km^{-1})	S_{liq} ($\mu m^2/cm^3$)	S_{sol}	V_{liq} ($\mu m^3/cm^3$)	V_{sol}
0^{abcd}	198	0	1.06	1.3	0.20	$5.0 \cdot 10^{-4}$	1.43	0.0	$9.0 \cdot 10^{-2}$	0.0
3^{ab}	188	0	2.48	0.6	0.52	$9.3 \cdot 10^{-3}$	13.3	0.0	2.3	0.0
3^{cd}	184	0	1.26	1.1	0.29	$2.4 \cdot 10^{-3}$	4.1	0.0	0.4	0.0
9^{ab}	186	0	3.41	0.4	0.62	$1.2 \cdot 10^{-2}$	16.7	0.0	3.4	0.0
9^{cd}	182	0	1.39	1.0	0.35	$3.4 \cdot 10^{-3}$	5.4	0.0	0.6	0.0
18^{a}	186	80	19.0	47.4	1.48	$5.7 \cdot 10^{-2}$	0.26	96.9	$9.4 \cdot 10^{-3}$	47.8
18^{b}	186	0.1	5.71	25.1	5.28	$1.7 \cdot 10^{-2}$	13.8	13.6	2.6	45.5
18^{c}	182	70	10.8	45.5	1.10	$3.9 \cdot 10^{-2}$	0.18	66.8	$4.5 \cdot 10^{-3}$	24.6
18^{d}	182	0.2	2.63	29.1	5.50	$7.1 \cdot 10^{-3}$	2.3	11.4	0.2	24.9
33^{a}	188	80	3.49	36.0	0.52	$1.0 \cdot 10^{-2}$	0.16	13.6	$4.7 \cdot 10^{-3}$	2.4
33^{b}	188	0.1	1.90	5.0	1.06	$4.0 \cdot 10^{-3}$	5.3	1.3	1.0	1.3
33^{c}	184	70	1.55	18.6	0.31	$3.9 \cdot 10^{-3}$	0.14	5.4	$3.4 \cdot 10^{-3}$	0.6
33^{d}	184	0.2	1.25	7.4	0.64	$1.2 \cdot 10^{-3}$	2.0	0.8	$1.5 \cdot 10^{-1}$	$4.5 \cdot 10^{-1}$
44^{a}	192	80	3.21	34.9	0.53	$9.0 \cdot 10^{-3}$	0.04	12.1	$5.1 \cdot 10^{-4}$	2.1
44^{b}	192	0.1	1.37	9.6	1.65	$1.6 \cdot 10^{-3}$	2.0	1.5	0.2	1.7
44^{c}	187	70	1.5	17.6	0.30	$3.5 \cdot 10^{-3}$	0.09	5.0	$1.8 \cdot 10^{-3}$	0.5
44^{d}	187	0.2	1.22	7.0	0.65	$1.1 \cdot 10^{-3}$	1.8	0.8	0.1	0.4
55^{a}	198	80	1.07	4.6	0.20	$6.0 \cdot 10^{-4}$	0.03	1.4	$3.5 \cdot 10^{-4}$	$8.8 \cdot 10^{-2}$
55^{b}	198	0.1	1.09	2.1	0.24	$5.4 \cdot 10^{-4}$	1.5	0.01	0.1	$1.0 \cdot 10^{-2}$
55^{c}	198	70	1.09	5.4	0.20	$6.7 \cdot 10^{-4}$	0.06	1.5	$7.7 \cdot 10^{-4}$	$9.8 \cdot 10^{-2}$
55^{d}	198	0.2	1.08	2.5	0.20	$5.0 \cdot 10^{-4}$	1.4	0.08	$7.8 \cdot 10^{-2}$	$1.5 \cdot 10^{-2}$

(*) Indices *a* and *b* indicate 1000 K/day and 10 K/day simulations for 4 ppmv H_2O-10 ppbv HNO_3, respectively. Indices *c* and *d* indicate 1000 K/day and 10 K/day simulations for 2 ppmv H_2O-2 ppbv HNO_3, respectively [9]. NUC stands for percent of particles nucleated. R and D are the backscatter and depolarization ratios, while EXT is the 532 nm extinction coefficient. S_{liq}, and S_{sol} represent the surface area of liquid and solid particles, respectively. V_{liq}, and V_{sol} represent the volume of liquid and solid particles, respectively.

4 K lower than the present one, due to depression in equilibrium temperatures of depleted species.

3·1. *Temperature history.* – The air parcel temperature history, together with the equilibrium temperatures of NAT and ice are plotted in fig. 1a. To study the response time and equilibrium values of the investigated parameters, fast temperature changes followed by a long stabilization time have been adopted. In the upper part of fig. 1a are also indicated the species which are stable during the corresponding time interval. Simulations start with a first cooling to 188 K which puts the air parcel into a STS stability region for 3 hours (equilibrium reached at $t = 3$ h). The following cooling to 186 K leads the STS below the ice frost point, where temperature is kept constant for 5 hours ($t = 9$ h). No nucleation is observed at this temperature. Homogeneous nucleation is then induced by further cooling: in one run at 1000 K/day (open symbols) and in the other one at 10 K/day (full symbols). The two runs lead, respectively, to the nucleation of 80% and 0.1% of ambient particles ($N_0 = 10\ cm^{-3}$), the larger sizes nucleating first. Once nucleation takes place, the air parcel is warmed and kept at 186 K, *i.e.*, within a stability point for ice, STS, NAT, and SAT, for at least 5 hours ($t =$ 18 h). A second warming to 188 K leads then into a stability region for STS, NAT, and

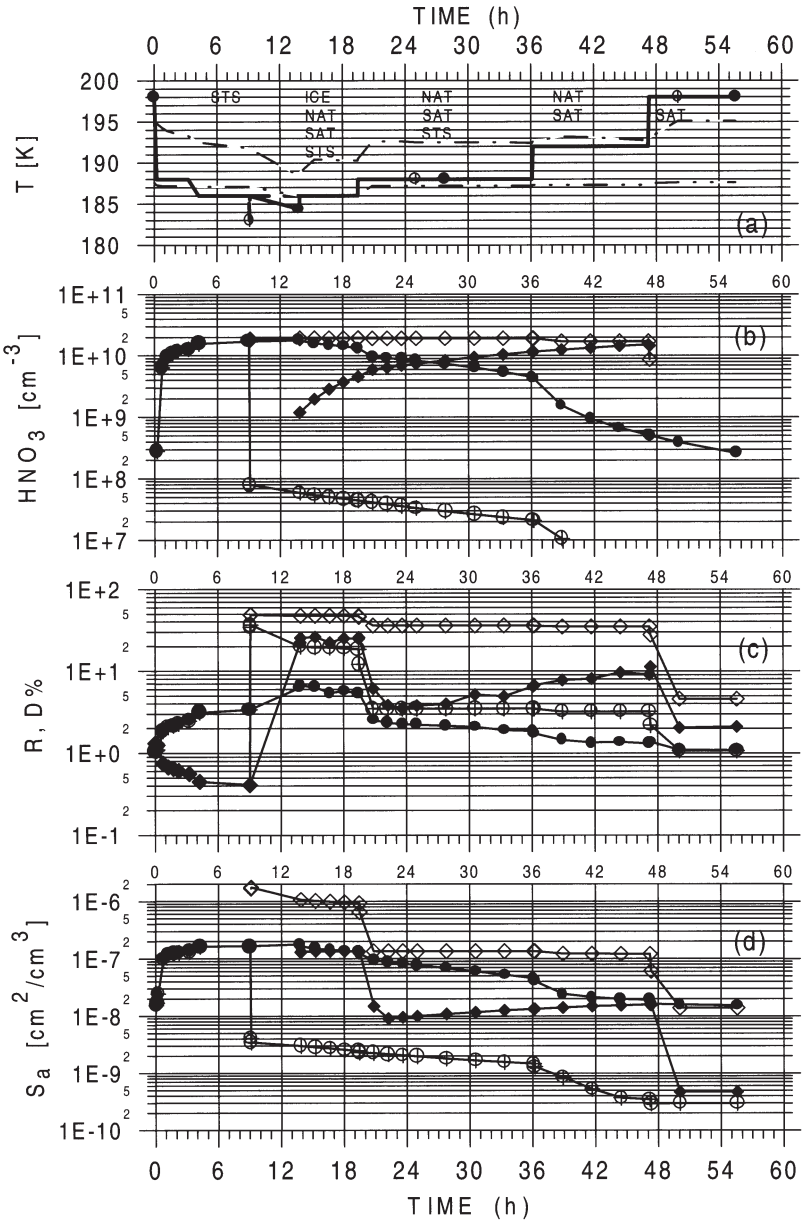

Fig 1. – a) Time history of the modeled air parcel temperature. Starting at $t = 9$ h two cooling rates are employed: 1000 K/day (crossed circles) and 10 K/day (full circles), respectively. Dash-dotted and dash-double dotted lines represent NAT and ice equilibrium temperatures, respectively. In all plots open symbols refer to the 80% (1000 K/day) nucleation level, full symbols to the 0.1% (10 K/day) level. b) Time evolution of the HNO_3 content in the liquid (circles) and solid (diamonds) phases of simulated mixed-phase PSC. c) Time evolution of the parallel backscatter ratio R (circles) and depolarization ratio D (diamonds) in the modeled air parcel. d) Time evolution of particles surface area S_a for both liquid (circles) and solid (diamond) phases in the modeled air parcel.

SAT alone for 16 hours ($t = 33$ h). The following rise to 192 K puts the air parcel into a NAT and SAT stability temperature for 11 hours ($t = 44$ h). Finally, temperature is increased and kept for 9 hours at 198 K, where SAT only is stable ($t = 55$ h).

For both liquid and solid phases the time evolution of particles HNO_3 content, of their backscatter and depolarization ratio, and of their surface area is plotted in figs. 1b, 1c and 1d, respectively.

3·2. *Formation of* STS *and nucleation of ice.* – Figure 1b shows STS condensation at 188 K to proceed with a typical (1/e) HNO_3 depletion time of approximately 3 hours. At 186 K, about 90% of the ambient HNO_3 (1.94×10^{10} molecules/cm^3) condensed into STS. Formation of STS changes the backscatter ratio from background values of 1.06 to $R = 2.5$ at 188 K and $R = 3.4$ at 186 K (fig. 1c). At the same time, the increased backscatter from spherical non-depolarizing particles leads to a decrease in the depolarization ratio from the molecular value $D = 1.4\%$, down to $D \approx 0.6\%$ at 188 K and $D \approx 0.4\%$ at 186 K. These R and D values are compatible with type 1b PSC [18]. The STS surface area is of the order of 13 μm^2/cm^3 at 188 K and 17 μm^2/cm^3 at 186 K.

Synoptic and wave-type cooling to the nucleation point starts at $t \approx 9$ h. Ice homogeneous nucleation takes place between 185.12 and 184.08 K in the 1000 K/day case and between 185.12 and 184.81 K in the 10 K/day case. Respectively, 7.9 and 1×10^{-2} crystals/cm^3 are generated out of the ambient 10 particles/cm^3, *i.e.*, approximately 80% and 0.1% of the total. It is interesting to note how the NAT heterogeneous nucleation levels computed in [14] were of the order of 80% at approximately 50 K/day, while levels below 1% were only obtained for cooling rates of 0.5 K/day. However, it should be remembered that the heterogeneous nucleation rates strongly depend on the poorly known "contact angle" parameter [14].

3·3. *Fast cooling case.* – The large difference in nucleated particles resulting from the two cooling cases addressed here strongly influences the physical and optical properties of the ice and NAT aerosols evolving after nucleation. Accordingly with the assumption that NAT forms on the nucleated ice particles, fig. 1b shows that in the air parcel cooled at 1000 K/day most of the ambient HNO_3 forms the NAT solid phase until temperature reaches above the NAT equilibrium point ($t = 47$ h). As in this case most background particles nucleate and grow, both backscatter and depolarization ratios reach maximum values compatible with the given mixing ratios: $R \approx 19$ and $D \approx 47\%$ for ice (plus NAT and SAT) at 186 K and $t = 18$ h ($R \approx 40$, $D = 50\%$ were reached just after nucleation at 183 K), and $R = 3.5$–3.2 and $D \approx 35\%$ for NAT (plus SAT) at $T =$ 188–192 K (fig. 1c, and table I). These values show that when NAT nucleates on most background aerosols the backscatter ratio is slightly larger but comparable to the STS case, *i.e.*, type 1b PSC, while depolarization ratios match the ones of type 1a PSC [18].

3·4. *Slow cooling case.* – In the 10 K/day cooling case, 0.1% particles nucleate at $t \approx$ 14 h. After this point, it takes approximately 12 hours for the liquid and solid phases to reach the same content in HNO_3 at $t = 26$ h, and over 30 hours to transfer the nitric acid initially condensed into the STS phase to NAT crystals (fig. 1b). The total surface area is always smaller in the case of selectively nucleated size distributions with respect to highly nucleated ones (fig. 1d). Consequently, the maximum backscatter and depolarization ratios are $R \approx 6$ and $D \approx 25\%$ for ice (plus NAT, STS and SAT at $t = 18$ h), $R \approx$ 2.2 and $D \approx 3\%$ at $t = 24$ h (non-equilibrium NAT+STS plus SAT) and $R \approx 1.4$, $D \approx 10\%$

at $t = 44$ h, for near-equilibrium NAT+STS (and SAT). These latter R values are small if compared to the scattering potential of NAT (*e.g.*, the fast cooling case), but are typical of solid, HNO_3-based PSC type 1a [18]. The corresponding D values are compatible with the ones indicated for type 1a PSC, when molecular contribution is subtracted as done in [18]. Such a combination of low backscatter and depolarization ratios is frequently detected by lidar observations of HNO_3-based PSC over Antarctica [9].

The final warming of the modeled air parcel to a stability point of SAT alone ($T = 198$ K at $t = 47$ h) leads in both simulations to values of $R \approx 1.08$, while $D = 2.1\%$ for 0.1% particles nucleated and $D = 4.6\%$ for 80% particles nucleated (fig. 1c, and table I).

3·5. *Further comparisons.* – Size distributions obtained at $t = 0$, 19 and 44 h for the two runs are presented in fig. 2. At these times distributions are representative of background aerosols, ice and NAT PSC, respectively. Since in the 10 K/day case only a few particles grow (specifically the ones located in bins of the background distribution with $r > 0.5$ μm, *e.g*, fig. 2b), these reach typical sizes of the order of $r \approx 10$ μm in the case of ice at 186 K ($t = 19$ h), and $r \approx 3.5$ μm for NAT at both 188 K ($t = 33$ h) and 192 K ($t = 44$ h). These sizes convert to settling times of 1 day/km and 8 day/km, respectively. Conversely, in the 1000 K/day case, the largest size reached by the distribution bin with initial radius $r = 0.5$ μm (which grew to the largest sizes in the previous case) is $r \approx 3$ μm for ice at 186 K and $r \approx 1.5$ μm for NAT at 188 and 192 K, respectively (*e.g.*, fig. 2a). In this case the ice particles would settle at a lower speed than NAT selectively nucleated at 10 K/day would do, while NAT particles would show a settling time of approximately 28 days/km.

The 0.1% selective nucleation case also shows how surface area of mixed-phase PSC can be dominated by the STS liquid phase even in the presence of ice (fig. 1d at $t =$ 14–19 h). In fact, the liquid phase provides the largest surface area also during the long non-equilibrium period $t = 20$–47 h, even when most of the nitric acid has been transferred to NAT. In this case, liquid surfaces in excess of 5 $\mu m^2/cm^3$ are still present 20 hours past the nucleation of NAT. This behavior indicates that along with rapid

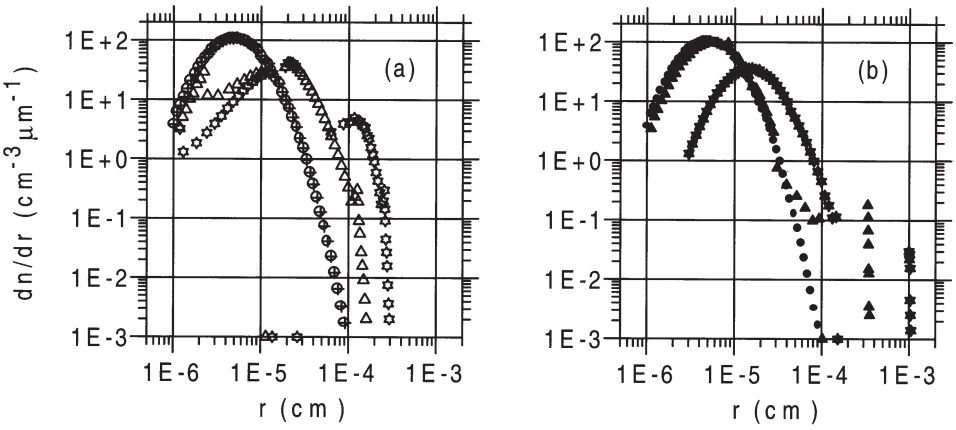

Fig. 2. – Model-derived size distributions: a) 1000 K/day cooling case (open symbols) and b) 10 K/day cooling case (full symbols). Circles show the initial ($t = 0$), lognormal size distribution. Stars describe the size distribution at $t = 19$ h, when ice at equilibrium is the dominating species. Triangles represent the distribution at $t = 44$ h, when NAT is dominating.

removal of crystalline HNO_3 by sedimentation of the solid component, mixed-phase PSC can retain a large potential for halogen activation by heterogeneous chemistry processes developing on the surface of their liquid particles.

Some further considerations can be drawn from the results of simulations for a denitrified and dehydrated atmosphere and from the distribution effective radius r_{eff} presented in table I: 1) the PSC effective radii are mostly in excess of $r_{\text{eff}} = 0.5$ μm, supporting therefore the assumption of a constant fractional depolarization employed in the model to compute D; 2) the distribution effective radius is much larger in the case of selective nucleation than for full nucleation; 3) condensation of ice in a dehydrated atmosphere leads to R and D values similar to the ones of NAT in non-depleted conditions.

4. – Conclusions

Optical and physical properties of polar stratospheric clouds have been computed by means of a numerical model simulating the microphysics of homogeneous nucleation and growth of stratospheric aerosols. At 50 hPa, 10 ppbv HNO_3 and 4 ppmv H_2O, the two cooling rates addressed (1000 and 10 K/day) led to the nucleation of 80% and 0.1% of the background aerosols, respectively. The first case compares well with lee-wave PSC observations [6], the latter with cirrus nucleation levels. STS reach a backscatter ratio of the order of $R \approx 3.5$, while the depolarization ratio D decreases below molecular levels. The 0.1% nucleated PSC show small values of R and medium-low values of D, while the 80% nucleation case presents the highest values of both R and D. While STS PSC fit well the type 1b PSC characteristics as defined in [18], only the 0.1% nucleation case is compatible with the type 1a PSC characteristics in the case of NAT-STS PSC. This behaviour indicates that the commonly used classification into type 1a or 1b PSC is too general and cannot represent the actual phase and composition of PSC. The presented results also substantiate the hypothesis [23] that selectively nucleated NAT particles can grow large enough (typical value found here: 3.5 μm in radius) to generate in a few weeks the conditions of denitrification without large dehydration observed in the late winter polar stratosphere. Moreover, the liquid phase surface area of these PSC can remain large enough (above 5 $\mu m^2/cm^3$) to allow for heterogeneous activation of halogens to proceed even after nucleation and during settling of NAT and/or ice particles. This action can extend even further if settling removes the competing NAT crystals from the air mass. The change in homogeneous nucleation level determined by the two cooling rates employed in this exercise leads to believe that HNO_3-based PSC are likely to present a continuum of R and D combinations, strongly dependent on the air parcel thermal history.

* * *

This work was partly supported by the Italian Space Agency, ASI.

REFERENCES

[1] *WMO, Scientific assessment of ozone depletion: 1994*, World Meteorological Organization, Global Ozone Research and Monitoring Project, Report No. 37, Geneva, 1995.

[2] TABAZADEH A., TURCO R. P. and JACOBSON M. Z., *A model for studying the composition and chemical effects of stratospheric aerosols, J. Geophys. Res.*, **99** (1994) 12897-12914.

[3] HANSON D. R. and MAUERSBERGER K., *Laboratory studies of the nitric acid trihydrate, implications for the south polar stratosphere, Geophys. Res. Lett.*, **15** (1988) 855-858.
[4] SANTEE M. L., TABAZADEH A., MANNEY G. L., SALAWITCH R. J., FROIDEVAUX L., READS W. G. and WATERS J. W., *UARS MLS HNO_3 observations: Implications for Antarctic PSCs, J. Geophys. Res.*, **103** (1998) 285; 313.
[5] FOX L.E., WORSNOP D. R., ZAHNISER M. S. and WOFSY S. C., *Metastable phases in polar stratospheric aerosols, Science*, **267** (1995) 351-355.
[6] CARSLAW K. S., WIRTH M., TSIAS A., LUO B. P., DORNBRACK A., LEUTBECHER M., VOLKERT H., RENGER W., BACMEISTER J. T. and PETER T., *Particle microphysics and chemistry in remotely observed mountain polar stratospheric clouds, J. Geophys. Res.*, **103** (1998) 5785-5796.
[7] DYE J. E. *et al.*, *In-situ observations of an Antarctic polar stratospheric cloud: similarities with Arctic observations, Geophys. Res. Lett.*, **23** (1996) 1913-1916.
[8] GOODMAN J., TOON O. B., PUESCHEL R. F., SNETSINGER K. G. and VERMA S., *Antarctic stratospheric ice crystals, J. Geophys. Res.*, **94** (1989) 16449-16457.
[9] GOBBI G. P., DI DONFRANCESCO G. and ADRIANI A., *Physical properties of stratospheric clouds during the Antarctic winter of 1995, J. Geophys. Res.*, **103** (1998) 10859-10874.
[10] PRUPPACHER H. R. and KLETT J. D., *Microphysics of clouds and precipitation* (D. Reidel) 1978.
[11] MEILINGER S. K., KOOP T., LUO B. P., HUTHWELKER T., CARSLAW K. S., KRIEGER U., CRUTZEN P. J. and PETERC T., *Size-dependent stratospheric droplet composition in lee wave temperature fluctuations and their potential role in PSC freezing, Geophys. Res. Lett.*, **22** (1995) 3031-3034.
[12] TSIAS A., PRENNI A. J., CARSLAW K. S., ONASCH T. P., LUO B. P., TOLBERT M. A. and PETER T., *Freezing of polar stratospheric clouds in orographically induced strong warming events, Geophys. Res. Lett.*, **24** (1998) 2303-2306.
[13] PINNICK R. G., ROSEN J. M. and HOFMANN D. J., *Stratospheric aerosol measurements, III, Optical model calculations, J. Atmos. Sci.*, **33** (1976) 304-314.
[14] WOFSY S. C., GOBBI G. P., SALAWITCH R. J. and MCELROY M. B., *Nucleation and growth of HNO_3-$3H_2O$ particles in the polar stratosphere, J. Atmos. Sci.*, **47** (1990) 2004-2012.
[15] JENSEN E. J. *et al.*, *Microphysical modeling of cirrus, 1: Comparison with 1986 FIRE IFO measurements, J. Geophys. Res.*, **99** (1994) 10421.
[16] TOON O. B., TURCO R. P., JORDAN J., GOODMAN J. and FERRY G., *Physical processes in polar stratospheric clouds, J. Geophys. Res.*, **94** (1989) 11359-11380.
[17] YOUNG K. C., *Microphysical processes in clouds* (Oxford University Press, New York) 1993.
[18] BROWELL E. V., BUTLER C. F., ISMAIL S., ROBINETTE P. A., CARTER A. F., HIGDON N. S., TOON O. B., SHOEBERL M. R. and TUCK A. F., *Airborne lidar observations in the wintertime Arctic Stratosphere: 1. Polar stratospheric clouds, Geophys. Res. Lett.*, **17** (1990) 385-388.
[19] SASSEN K., *Air-truth lidar polarization studies of orographic clouds, J. Appl. Met.*, **17** (1978) 73-91.
[20] MISHCHENKO M. I. and SASSEN K., *Depolarization of lidar returns by small ice crystals: An application to contrails, Geophys. Res. Lett.*, **25** (1998) 309-312.
[21] MURPHY D. M. and GARY B. L., *Mesoscale temperature fluctuations and polar stratospheric clouds, J. Atmos. Sci.*, **52** (1995) 1753-1760.
[22] GOBBI G. P., *Modeling optical properties of mixed-phase polar stratospheric clouds in late winter conditions*, in *Proc. SIF*, edited by H. COLACINO, G. GIOVANELLI and L. STEFANUTTI, vol. **62** (Editrice Compositori, Bologna) 1998, p. 283.
[23] SALAWITCH R. J., GOBBI G. P., WOFSY S. C. and MCELROY M. B., *Denitrification of the Antarctic stratosphere, Nature*, **339** (1989) 525-527.